ROBUST CONTROL OF TWO-WHEELED ROBOT: THEORETICAL AND EXPERIMENTAL EVALUATION

TSONYO N. SLAVOV[1], JORDAN K. KRALEV[1], PETKO H. PETKOV[2*]

[1]*Department of Systems and Control, Technical University of Sofia,*
1157 Sofia, Bulgaria
e-mails: ts.slavov@tu-sofia.bg, j.kralev@tu-sofia.bg

[2]*Department of Engineering Sciences, Bulgarian Academy of Sciences,*
1040 Sofia, Bulgaria
e-mail: php@tu-sofia.bg

Abstract. In this paper, we survey some recent results related to the identification, design, and experimental evaluation of a robust control system intended for vertical stabilization and tracking of the desired horizontal trajectory of a two-wheeled robot. A single-input multi-output uncertainty model is utilized, obtained by an appropriate identification procedure. Results of the theoretical and experimental comparison of two controllers are presented: an LQG controller including a Kalman filter and a μ-controller ensuring robust stability and robust performance of the closed-loop system. Both controllers are embedded in a Raspberry Pi 4B microcontroller. The results of the closed-loop system experimental evaluation confirm the fulfillment of the design requirements.

Keywords: two-wheeled robot; robust control; LQG control; μ-control

1. INTRODUCTION

The control of two-wheeled robots has remained an intensive research topic in recent years, see for instance [2, 3, 10, 13, 15, 19, 20]. Due to the inherent instability- ity of the plant, the precise robot control requires to know sufficiently accurate dynamical model that takes into account the parameter uncertainties and disturbances in the plant, sensors, and actuators. For this aim, it is appropriate to use a closed-loop Single-Input Multi-Output (SIMO) identification method, which yields a low-order linear small deviations model. The uncertain robot model is derived from experimental results as described in [8, 15, 19, 20]. As a result of such modeling, one obtains the robot dynamics description in the form

* Corresponding author
http://doi.org/10.7546/EngSci.LXII.25.02.01

of Linear Fractional Transformation (LFT) that reflects the integral effect of plant uncertainties. This LFT is used in the controller design and in the time-domain and frequency-domain analysis of the closed-loop system.

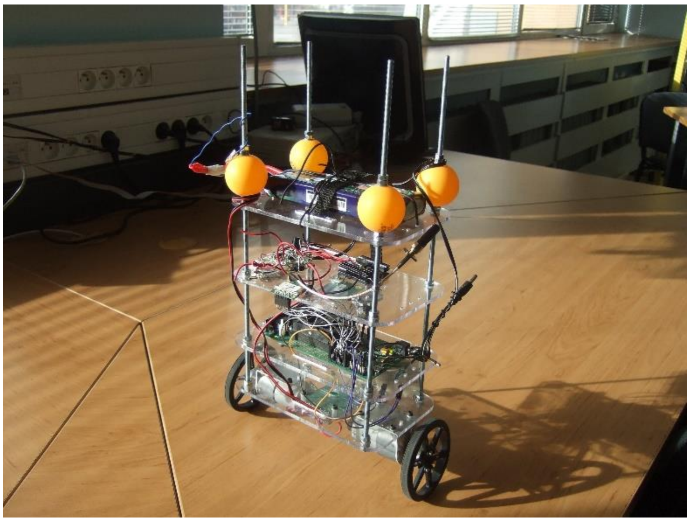

Fig. 1. Robot View

In this paper, we survey some recent results obtained by the authors that are related to the identification, design, and experimental evaluation of a robust control system intended for stabilization of a two-wheeled robot in the vertical plane and tracking the desired trajectory in the horizontal plane. The paper presents experimentally confirmed results concerning the precise robot control, implementing two different controllers. A single-input multi-output uncertainty model is utilized, obtained by an appropriate identification procedure described in [11, 12]. For this aim, we use the model derived in [19], which was previously implemented in the robot controller design [20]. Two controllers are theoretically and experimentally compared: an LQG controller including a Kalman filter and a μ-controller ensuring robust stability and robust performance of the closed-loop system. Both controllers are embedded in a Raspberry Pi 4B microcontroller, and results from the closed-loop system experimental evaluation confirming the design are presented.

The paper contains eight sections. In section 2, we provide a brief description of the two-wheeled robot constructed by the authors, referring the reader to the paper [15] for more detailed information. The uncertain 5th order Single-Input Two-Output (SITO) robot model derived in [19] is presented in section 3. In section 4, we describe the LQG design involving LQR design and design of a Kalman filter [19]. Section 5 is devoted to the design of a μ-controller ensuring guaranteed closed-loop robust stability and robust performance [20]. In sect. 6, we compare the frequency responses and robustness properties of the closed-loop system for both controllers. In section 7, we present the results obtained from the experimental comparison of the two controllers, and in section 8, we give some conclusions.

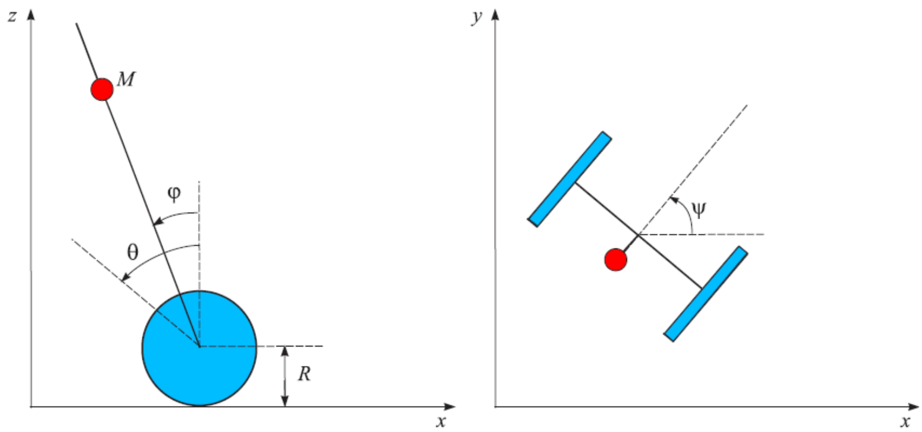

Fig. 2. Robot motion in the vertical (left) and horizontal (right) plane

2. ROBOT DESCRIPTION

The robot view is shown in Fig. 1, and a schematic diagram of the two-wheel robot motion in both planes is presented in Fig. 2. The deviation of the robot position from the vertical position is characterized by the tilt angle ϕ and its motion in the horizontal plane can be described by the angle $\theta = (\theta_L + \theta_R)/2$ describing the average wheel's motion, where θ_L and θ_R denote the angle position of the left and right wheel angles. The motion of the robot with respect to the vertical axis is steered by a separate simple controller and is not considered here.

The robot control system consists of two servo motors for wheel actuation, a MEMS inertial sensor measuring the angular velocity $\dot{\phi}$ of the robot body, quadrature encoders measuring the wheel's position, and a digital controller in which a discrete real-time stabilization algorithm is implemented. The MEMS gyro sensor is characterized by a large drift. The sampling period of the control action is equal to $T_s = 0.005\ s$. The balancing of the robot is achieved by rotating the wheels in the appropriate direction. The calculation of the control inputs to both DC drive motors is done in single precision (32 bits) based on signals from the MEMS sensor that measures the rate $\dot{\phi}$ (an estimate of the angle ϕ is obtained by integrating $\dot{\phi}$) and signals from the rotary encoders measuring the wheel's rotation angle θ. The control of the DC brushed motors is realized by Pulse Width Modulated (PWM) signals.

3. THE UNCERTAIN MODEL

In this paper, we implement an estimated SITO state-space model of the wheel's dynamics and robot motion, whose input is the control action u to the DC motors, and the outputs are the wheel's angular rate $\dot{\theta}$ and the tilt angle ϕ of the robot body. This model was already used in [19, 20] for other types of controller design. A disadvantage of this model is that, as a result of the identification, it has a large number of structural uncertainties, making its implementation unfeasible. Hence, it is appropriate to use transfer function models $G_{\dot{\theta}u}$ and $G_{\phi u}$

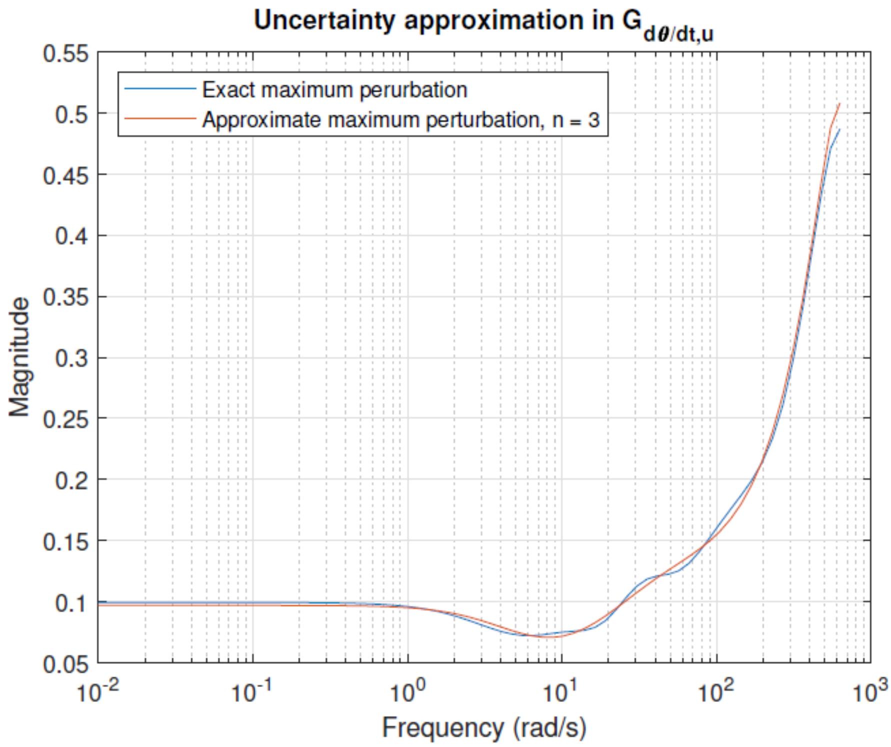

Fig. 3. Approximation of the relative uncertainty in $G_{\dot{\theta}u}$

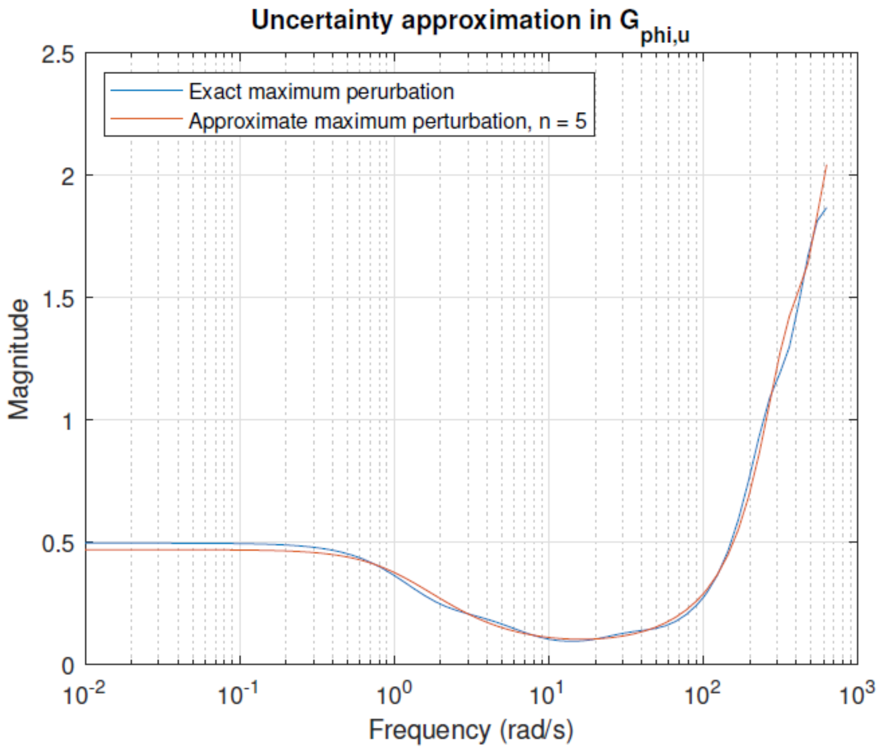

Fig. 4. Approximation of the relative uncertainty in $G_{\phi u}$

that contain complex (unstructured) uncertainties [7]. Note that this is associated with the introduction of some conservatism in the model, but allows to find lower-order controllers. Exploiting the parameter confidence intervals obtained by the identification, we obtain the maximum relative deviations from the nominal model in the frequency domain. Assuming the presence of output unstructured uncertainties, we can approximate these deviations by using an optimization procedure of given order shaping filters. The maximum relative uncertainties in $G_{\dot{\theta} u}$ and $G_{\phi u}$ along with their approximations, are represented in Fig. 3 and 4, respectively. Note that the maximums of the uncertainties are in the higher frequency range, which means that the model is more accurate in the low and middle frequency range. The approximations are used to determine the weighting shaping filters in the corresponding output multiplicative uncertainty representations. It should be pointed out that in the given case, it is advantageous to use output instead of input uncertainties to find the corresponding minimal state-space realizations. These filters are represented by 3rd order transfer functions. As a result of the identification procedure, the nominal 5th-order discrete-time state space model of the robot is obtained as

$$x_{k+1} = Ax_k + Bu_k + K_e e_k, \tag{1}$$

$$y_k = Cx_k + Du_k + e_k,$$

where $x_k, u_k, y_k = [\dot{\theta}, \phi]^T$ and $e_k = [e_{\dot{\theta}}, e_{\phi}]^T$, are the state, input, output, and residue error vectors, respectively. The model matrices A, B, C, D, K_e in the observable canonical form are:

$$A = \begin{bmatrix} 0 & 1 & 0 & 0 & 0 \\ -7.0976 \cdot 10^{-1} & 1.6834 \cdot 10^{0} & -7.9018 \cdot 10^{-1} & 9.9694 \cdot 10^{-2} & 7.6250 \cdot 10^{-1} \\ 0 & 0 & 0 & 1 & 0 \\ 0 & 0 & 0 & 0 & 1 \\ -2.9747 \cdot 10^{-4} & 2.8183 \cdot 10^{-4} & 5.6080 \cdot 10^{-1} & -2.1149 \cdot 10^{0} & 2.5546 \cdot 10^{0} \end{bmatrix},$$

$$B = \begin{bmatrix} -3.8502 \cdot 10^{-3} \\ 1.6537 \cdot 10^{-1} \\ -1.2123 \cdot 10^{-5} \\ 5.8352 \cdot 10^{-5} \\ 2.2311 \cdot 10^{-4} \end{bmatrix}, \tag{2}$$

$$K_e = \begin{bmatrix} 8.3952 \cdot 10^{-1} & -5.1882 \cdot 10^{-1} \\ 7.4844 \cdot 10^{-1} & 5.9226 \cdot 10^{-1} \\ 1.6353 \cdot 10^{-4} & 1.8714 \cdot 10^{0} \\ 5.4093 \cdot 10^{-4} & 2.7881 \cdot 10^{0} \\ 1.0845 \cdot 10^{-3} & 3.3755 \cdot 10^{0} \end{bmatrix},$$

$$C = \begin{bmatrix} 1 & 0 & 0 & 0 & 0 \\ 0 & 0 & 1 & 0 & 0 \end{bmatrix},$$

$$D = \begin{bmatrix} 0 \\ 0 \end{bmatrix}$$

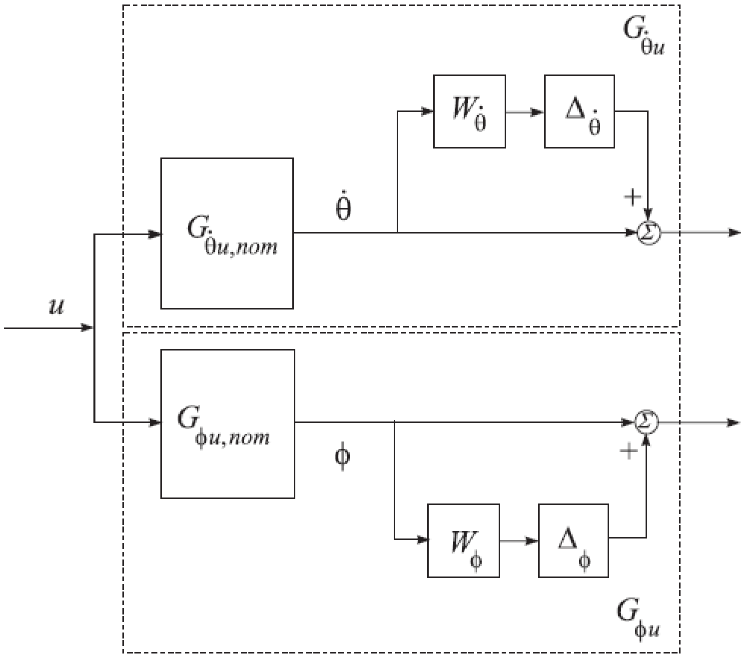

Fig. 5. Uncertain plant model

It is interesting that all open-loop poles of the model are unstable,

$$\lambda_1 = 0.5756, \lambda_2 = 0.9178, \lambda_3 = 0.8609, \lambda_4 = 0.9600, \lambda_5 = 1.0237.$$

The SITO uncertain model involving unstructured uncertainties is described by,

$$G_{\dot\theta u}(z) = \left(1 + W_{\dot\theta}(z)\Delta_{\dot\theta}\right)G_{\dot\theta u,nom}(z), \tag{3}$$

$$G_{\phi u}(z) = \left(1 + W_{\phi}(z)\Delta_{\phi}\right)G_{\phi u,nom}(z), \tag{4}$$

where $G_{\dot\theta u,nom}(z)$, $G_{\phi u,nom}(z)$, are the transfer functions of the nominal model derived from the state-space description (1), (2),

$$W_{\dot\theta}(z) = \frac{0.27680z^3 - 0.65150z^2 + 0.48620z - 0.11120}{z^3 - 1.66000z^2 + 0.50270z + 0.16010},$$

$$W_{\phi}(z) = \frac{0.83430z^3 - 1.82600z^2 + 1.25700z - 0.26200}{z^3 - 1.11800z^2 + 0.21280z - 0.08790}$$

are the 3rd-order shaping filters that represent the output multiplicative uncertainty and $\Delta_{\dot{\theta}}$, Δ_{ϕ} are the output multiplicative uncertainties that satisfy

$$\left|\Delta_{\dot{\theta}}\right| < 1, \left|\Delta_{\dot{\phi}}\right| < 1.$$

In Fig. 5, we show the model of the two-wheeled robot involving output multiplicative uncertainties. The order of the uncertain plant model is equal to 11.

In Fig. 6 and Fig. 7, we present families of frequency response plots corresponding to the uncertain models $G_{\dot{\theta}u}$ and $G_{\phi u}$.

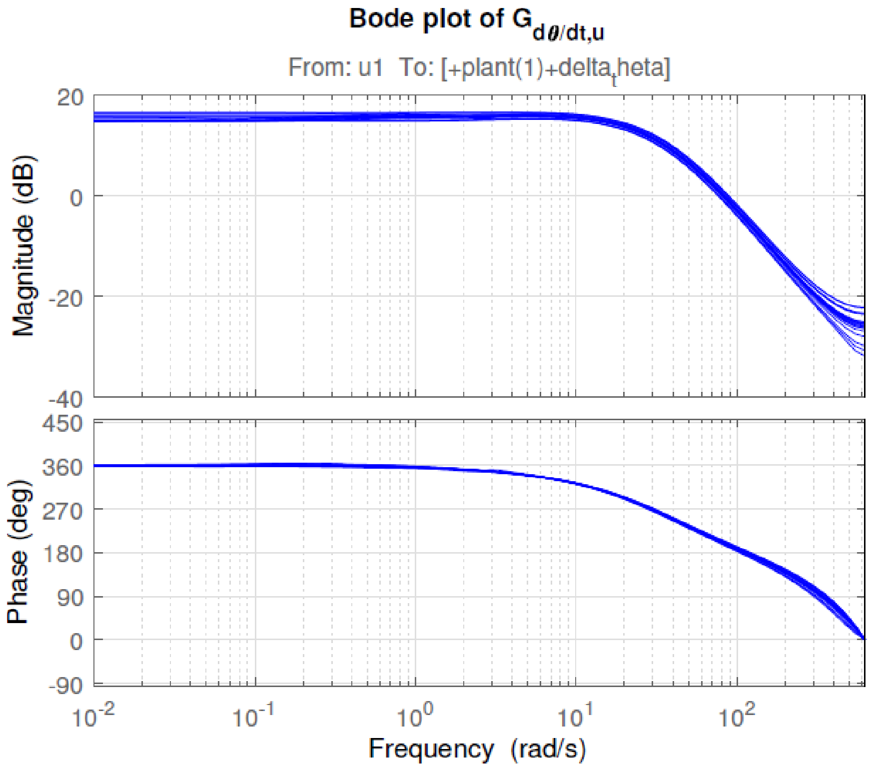

Fig. 6. The frequency responses corresponding to the uncertain transfer function $G_{\dot{\theta}u}$

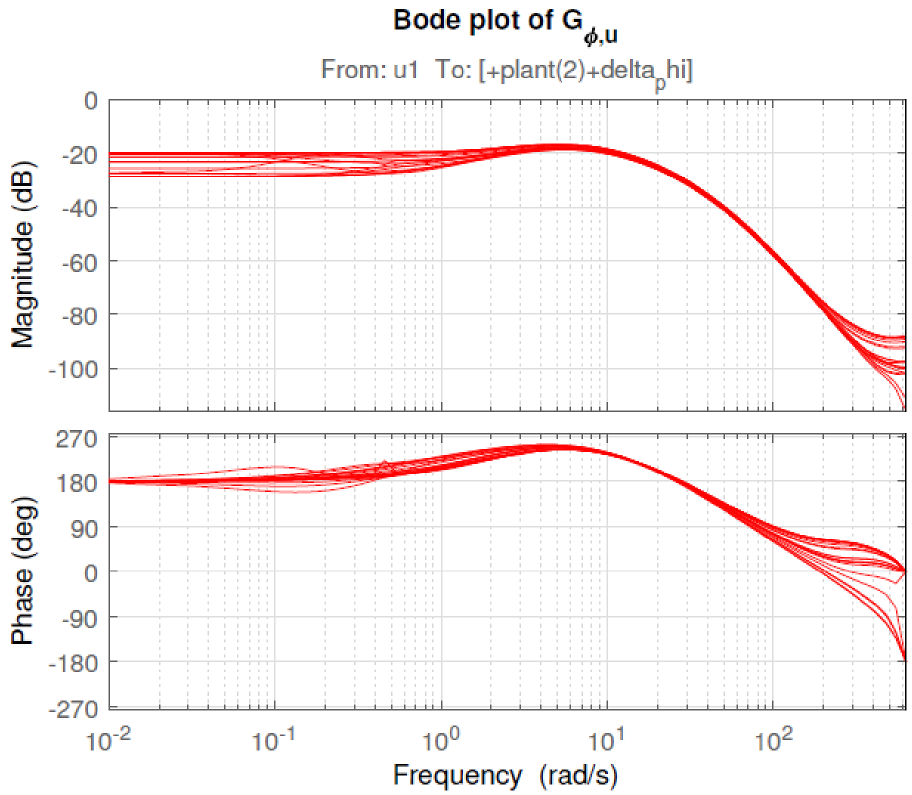

Fig. 7. The frequency responses corresponding to the uncertain transfer function $G_{\phi u}$

4. DESIGN OF LQG CONTROLLER

The LQG controller is frequently implemented for stabilization of two-wheeled robots, see for instance [3, 9, 18]. As it was shown in [10], the usage of a single-input single-output model of the robot in the design of such a controller leads to a closed-loop system that doesn't achieve robust performance. In this section, we shall design an LQG controller for the single-input two-output robot model that ensures both robust stability and robust performance of the closed-loop system. An important property of this controller is that its design takes into account the presence of large noise in the MEMS gyro.

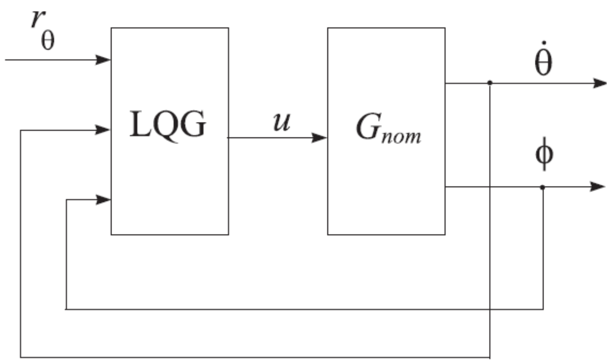

Fig. 8. System with LQG controller

The block diagram of the robot control system with an LQG controller is presented in Fig. 8, where G_{nom} is the nominal plant model is presented below. For the design of the LQG controller, the estimated state space model (1) is transformed by the MATLAB® function ss to the 5th order model

$$x(k+1) = Ax(k) + Bu(k) + J\nu(k), \tag{5}$$

$$y(k) = Cx(k) + H\nu(k)$$

where $\nu(k) = [\nu 1(k)\ \nu 2(k)]^T$ is a vector of white Gaussian noise with unit covariance. The fact that $\nu(k)$ is a white noise is due to the unbiased estimates of model parameters. The matrices A, B, C have the values shown in (2) and

$$J = \begin{bmatrix} 7.4683 \cdot 10^{0} & -6.5572 \cdot 10^{-3} \\ 6.6592 \cdot 10^{0} & 7.4854 \cdot 10^{-3} \\ 3.5072 \cdot 10^{-3} & 2.3653 \cdot 10^{-2} \\ 7.8700 \cdot 10^{-3} & 3.5237 \cdot 10^{-2} \\ 1.3350 \cdot 10^{-2} & 4.2662 \cdot 10^{-2} \end{bmatrix}, \qquad H = \begin{bmatrix} 8.8966 \cdot 10^{0} & 0 \\ 1.0967 \cdot 10^{-3} & 1.2639 \cdot 10^{-2} \end{bmatrix}$$

To provide robot stabilization in the vertical plane and to ensure tracking of the wheel position reference signal r_θ, it is appropriate to extend the model (5) with the additional states

$$x_\theta(k+1) = x_\theta(k) + T_0\dot{\theta}(k) = x_\theta(k) + T_0C_1x(k) + T_0H_1\nu(k) \tag{6}$$

$$x_{\int\theta}(k+1) = x_{\int\theta}(k) + T_0\big(r_\theta - \theta(k)\big) = x_{\int\theta}(k) + T_0r_\theta - T_0x_\theta(k)$$

$$-T_0^2C_1x(k) - T_0^2H_1\nu_1(k) \tag{7}$$

$$x_{\int\phi}(k+1) = x_{\int\phi}(k) - T_0\phi(k) = x_{\int\phi}(k) - T_0C_2(k) - T_0H_2\nu(k) \tag{8}$$

where $x_\theta(k)$ is the unmeasurable wheel position, obtained by numerical integration of $\dot{\theta}$, $x_{\int\theta}(k)$ is integral of the error in wheel position, $x_{\int\phi}(k)$ is the integral of the error in body tilt angle and C_1, H_1, C_2, H_2 are the first and the second rows of matrices C, H, respectively. Combining equations (5)-(8), for the description of the extended plant, one obtains

$$\bar{x}(k+1) = \bar{A}\bar{x}(k) + \bar{B}u(k) + \bar{J}v(k), \tag{9}$$

$$\bar{y}(k) = \bar{C}\bar{x}(k) + \bar{H}v(k)$$

where

$$\bar{x}(k) = [x_{\int\theta} x_{\int\phi} x_\theta x^T]^T$$

is the extended state vector, $\bar{y}(k) = [\theta\dot{\theta}\phi]^T$ is the extended output vector and

$$A = \begin{bmatrix} 1 & 0 & -T_0 & -T_0^2C_1 \\ 0 & 1 & 0 & -T_0C_2 \\ 0 & 0 & 1 & T_0C_1 \\ 0 & 0 & 0 & A \end{bmatrix}, \qquad \bar{B} = \begin{bmatrix} 0 \\ 0 \\ 0 \\ B \end{bmatrix}, \qquad \bar{J} = \begin{bmatrix} -T_0^2H_1 \\ -T_0H_2 \\ T_0H_1 \\ J \end{bmatrix},$$

$$\bar{C} = \begin{bmatrix} 0 & 0 & 1 & 0 \\ 0_{2\times1} & 0_{2\times1} & 0_{2\times1} & C \end{bmatrix}, \qquad \bar{H} = \begin{bmatrix} 0_{1\times2} \\ H \end{bmatrix}$$

4.1 LQR Design

In the design of the LQR controller, we use the deterministic part of the extended model (9). The design is performed to minimize the quadratic performance index

$$J(u)\sum_{k=0}^{\infty}[\bar{x}(k)^TQ\bar{x}(k) + u(k)^TRu(k)] \tag{10}$$

where Q and R are positive definite weighting matrices are chosen to ensure closed-loop system performance. The matrices Q and R are experimentally determined as

$$Q = \begin{bmatrix} Q_{\int\theta} & 0 & 0 & 0 \\ 0 & Q_{\int\phi} & 0 & 0 \\ 0 & 0 & Q_\theta & 0 \\ 0 & 0 & 0 & C^TQ_{\dot{\theta}\phi}C \end{bmatrix}, R = 100$$

where $Q_{\int\theta} = 30, Q_{\int\phi} = 25, Q_{\theta} = 1$, and

$$Q_{\dot{\theta}\phi} = \begin{bmatrix} 12 & 0 \\ 0 & 5 \end{bmatrix}$$

The optimal control law that minimizes (10) with respect to the system (9) is given by [5, Ch. 9]

$$u(k) = -K\bar{x}(k) \tag{11}$$

where the optimal feedback matrix K is determined by

$$K = (R + \bar{B}^T P\bar{B})^{-1}\bar{B}^T P\bar{A} \tag{12}$$

In (12), the matrix P is the positive definite solution of the discrete-time matrix algebraic Riccati equation

$$\bar{A}^T P\bar{A} - P - \bar{A}^T P\bar{B}(R + \bar{B}^T P\bar{B})^{-1}\bar{B}^T P\bar{A} + Q = 0 \tag{13}$$

The matrix K is computed by the function `dlqr` of MATLAB®.

4.2 Kalman Filter Design

Let the matrix K is partitioned as

$$K = \left[-K_{\int\theta} - K_{\int\phi} K_{\theta} K_{x}\right]. \tag{14}$$

according to the dimensions of the state vector elements $x_{\int\theta}, x_{\int\phi}, x_{\theta}, x$.

Since the plant states are unmeasurable, in practice the optimal control signal in equation (11) is evaluated from

$$u(k) = K_{\int\theta}\hat{x}_{\int\theta}(k) + K_{\int\phi}\hat{x}_{\int\phi}(k) - K_{\theta}\hat{x}_{\theta}(k) - K_{x}\hat{x}(k), \tag{15}$$

where $\hat{x}(k)$ is the estimate of the plant state $x(k)$. The estimates

$$\hat{x}_{\int\theta}(k), \hat{x}_{\int\phi}, x_{\theta}(k)$$

are calculated by using the approximate relationships

$$\hat{x}_{\theta}(k+1) = \hat{x}_{\theta}(k) + T_0\hat{\dot{\theta}}(k)), \tag{16}$$

$$\hat{x}_{\int\theta}(k+1) = \hat{x}_{\int\theta}(k) + T_0(r_{\theta}(k) - \hat{\theta}(k)),$$

$$\hat{\theta}(k) = \hat{x}_{\theta} \tag{17}$$

$$\hat{x}_{\int\phi}(k+1) = \hat{x}_{\int\phi}(k) - T_0\hat{\phi}(k) \tag{18}$$

The estimates $\hat{x}(k)$, $\hat{\dot{\theta}}(k)$ and $\hat{\phi}(k)$ are obtained by a Kalman filter. As customary for MEMS sensors, the gyroscope that measures body tilt rate $\dot{\phi}$ has significant noise ϕ_g. Its influence on body tilt angle ϕ is taken into account by the first-order model

$$\phi_g(k+1) = \phi_g(k) + T_0 J_g \nu_g(k), \tag{19}$$

where ν_g is a white Gaussian noise with unit variance, and the coefficient J_g is determined experimentally as $J_g = 0.0001$ to obtain a good estimate of ϕ_g. Combining equations (5) and (19), the Kalman filter design is performed for the extended system

$$x_f(k+1) = A_f x_f(k) + B_{fu}(k) + J_f \nu_f(k) \tag{20}$$

$$y_f(k) = C_f x_f(k) + H_f \nu_f(k)$$

where $x_f(k) = [x_k^T \phi_g(k)]^T$,$\nu_f = [\nu(k)\ \nu_g(k)]^T$ is a white Gaussian noise with covariance $D_{\nu f} = I$ and

$$A_f = \begin{bmatrix} A & 0 \\ 0 & 1 \end{bmatrix}, \qquad B_f = \begin{bmatrix} B \\ 0 \end{bmatrix}, \qquad J_f = \begin{bmatrix} J & 0 \\ 0 & T_0 J_g \end{bmatrix},$$

$$C_f = \begin{bmatrix} C_1 & 0 \\ C_2 & 1 \end{bmatrix}, \qquad H_f = [\, H \quad 0 \,]$$

A 6th-order discrete-time Kalman filter for the system (20) is obtained as [6, Ch.4]

$$\hat{x}_f(k+1) = A_f \hat{x}_f(k) + B_{fu}(k) + K_f(y_f(k+1) -$$

$$C_f B_{fu}(k) - C_f A_f \hat{x}_f(k)), \tag{21}$$

$$\hat{y}(k) = C_f \hat{x}_f(k)$$

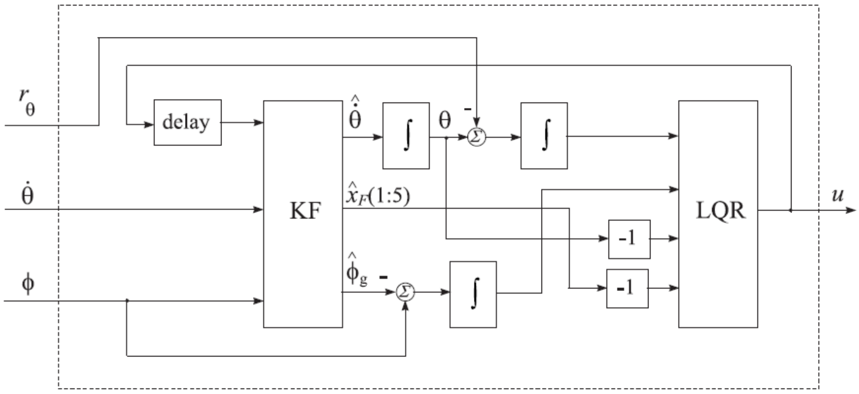

Fig. 9. Block diagram of the LQG controller

where $\hat{x}_f(k) = [\hat{x}(k)^T, \hat{y}(k) = [\hat{\dot\theta}(k)\ \hat{\phi}(k)]^T$, and $\hat{\phi}_g$ is an estimate of ϕ_g.

The block diagram of the LQG controller is shown in Fig. 9. The Kalman filter gain matrix K_f is determined as

$$K_f = D_\theta C_f^T (C_f D_\theta C_f^T + H_f D_{vf} H_f^T)^{-1} \tag{22}$$

where the matrix D_θ is obtained from the positive definite solution of the discrete-time matrix algebraic Riccati equation

$$Z = (I - K_f C_f) D_\theta (I - K_f C_f)^T + K_f H_f D_{vf} H_f^T K_f^T$$

$$\begin{aligned} D_\theta = (A_f - J_f D_{vf} H_f^T \big(H_f D_v H_f^T)^{-1} C_f\big) Z (A_f - \\ J_f D_{vf} H_f^T (H_f D_{vf} H_f^T)^{-1} C_f)^T + J_f D_{vf} J_f^T. \end{aligned} \tag{23}$$

The matrix K_f is computed by the function kalman of MATLAB®. The quantity $\hat{\phi}(k)$ which is used in the computation of the estimate (18), is obtained from

$$\hat{\phi}(k) = \phi(k) - \hat{\phi}_g(k) \tag{24}$$

where $\hat{\phi}_g(k)$ is the last element of the state estimate $\hat{x}_f$.

In Fig. 10, we show the magnitude plot of the LQG controller.

5. μ-CONTROLLER DESIGN

As is known, the purpose of the μ-controller is to ensure robust stability and robust performance of the closed-loop system in the presence of unstructured or structured dynamics [7, 17, 21].

The block diagram of the closed-loop system corresponding to the μ-synthesis problem is shown in Fig. 11, where r_θ is the wheel's reference angle and e_p, e_u are the weighted closed-loop system outputs. The aim of the controller K, determined by μ-synthesis, is to ensure robust stability and robust performance of the closed-loop system in the presence of the plant uncertainties Δ_θ and Δ_ϕ. To obtain better position accuracy, feedback from the integrated tracking error $err = r_\theta - \theta$ is introduced to the controller.

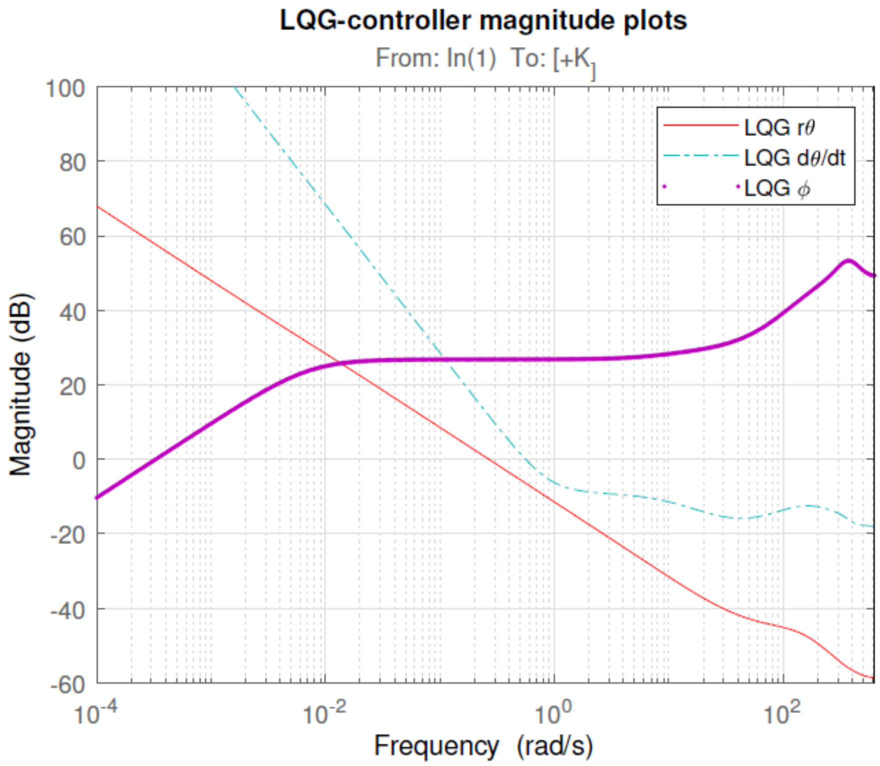

Fig. 10. LQG-controller magnitude plot

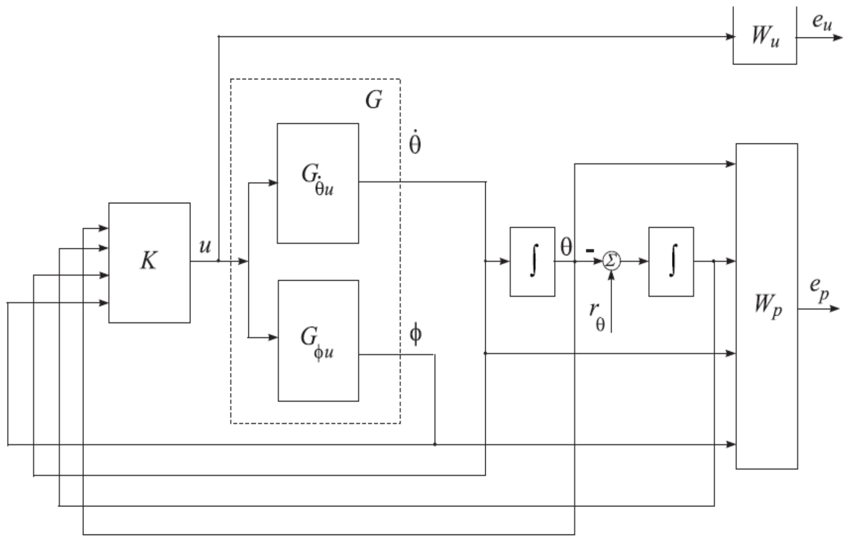

Fig. 11. Block diagram of the closed-loop system

The control action to the plant is implemented by a microcontroller in real-time, with the sampling frequency $f_s = 200\ Hz$. For this reason, the μ-synthesis is implemented to design a discrete-time controller at this sampling frequency.

Denote by

$$y_c = \left[\theta, \int (r_\theta - \theta), \dot\theta, \phi, \right]^T$$

the output feedback vector where $\int (r_\theta - \theta)$ is the result of the discrete-time integration of the difference $r_\theta - \theta$ using the forward Euler method. The controller transfer function matrix K is represented as

$$K = [K_\theta\ K_{\int err} K_{\dot\theta} K_\phi].$$

Then the control action is determined by the expression

$$\begin{aligned} u &= K y_c \\ &= K_\theta \theta + K_{\int err} \int (r_\theta - \theta) + K_{\dot\theta} \dot\theta + K_\phi \phi \end{aligned} \tag{25}$$

Using the notation

$$G_{\int}(z) = \frac{T_s}{z-1}, G_u(z) = \begin{bmatrix} G_{\int}(z)G_{\dot{\theta}u}(z) \\ -G_{\int}(z)^2 G_{\dot{\theta}u}(z) \\ G_{\dot{\theta}u}(z) \\ G_{\phi u} \end{bmatrix},$$

$$G_{r\theta}(z) = \begin{bmatrix} 0 \\ G_{\int}(z) \\ 0 \\ 0 \end{bmatrix},$$

where $T_s = 0.005$ s is the sampling period, the closed-loop system is described by the expressions

$$y_c = G_{r\theta} r_\theta + G_u u \tag{26}$$

$$u = K y_c \tag{27}$$

The weighted closed-loop system errors e_p and e_u satisfy the equation

$$\begin{bmatrix} e_p \\ e_u \end{bmatrix} = \begin{bmatrix} W_p S_o G_{r\theta} \\ W_u S_i K G_{r\theta} \end{bmatrix} r\theta \tag{28}$$

where $S_i = (1 - K G_u)^{-1}$ is the input sensitivity transfer function and $S_o = (I - G_u K)^{-1}$ is the output sensitivity transfer function matrix.

The performance criterion used in controller design requires that the transfer function matrix from the exogenous input signal r_θ to the output signals e_p and e_u to be small in the sense of $\|\cdot\|_\infty$, for all possible uncertain plant models. This leads to small weighted signals θ, $\int(r_\theta - \theta), \dot{\theta}$ and ϕ and small control action u in the desired frequency range. The transfer function matrices W_p and W_u reflect the relative importance of the different frequency ranges for which the performance requirements should be fulfilled [21].

The μ-synthesis is applied for several choices of performance weighting functions that ensure a good balance between system performance and robustness. Based on simulation and experimental results, the performance weighting function is chosen as low low-pass filter as (in the continuous-time case)

$$W_p(s)=$$
$$\begin{bmatrix} 0.5\dfrac{3s+1}{50s+1} & 0 & 0 & 0 \\ 0 & 4.7\dfrac{4s+1}{125s+1} & 0 & 0 \\ 0 & 0 & 0.7\dfrac{0.3s+1}{30s+1} & 0 \\ 0 & 0 & 0 & 0.75\dfrac{4s+1}{50s+1} \end{bmatrix}$$

The control weighting function is chosen as a high-pass filter with appropriate bandwidth to impose constraints on the spectrum of control actions [7]. In the given case, the control weighting function is chosen as a first-order filter as

$$W_u(s) = 0.4\frac{1}{30}\frac{s+1}{0.1s+1}$$

The weighting functions are discretized for the sampling period of 0.005 s and included in the open-loop system model.

The μ-synthesis is performed by using the Robust Control Toolbox®3 function **musyn** [1]. After the eighth iteration, the maximum value of μ is decreased to 0.503, and the final controller obtained is of 36th order. The controller order is reduced to 15th by using the command reduce of Robust Control Toolbox®3 without deterioration of the closed-loop performance.

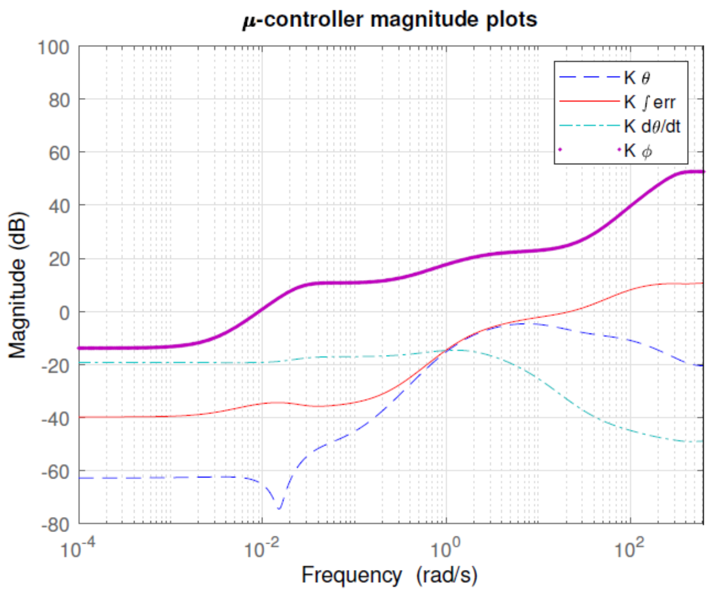

Fig. 12. μ-controller magnitude plot

The magnitude plots of K_θ, $K_{\int err}$, $K_{\dot{\theta}}$, and K_ϕ are shown in Fig. 12.

It is interesting that while the signal θ is multiplied by a gain less than one in the whole frequency range, the amplification of ϕ in the high frequency range is approximately 50 dB (more than 300 times), which emphasizes the importance of this variable in the stabilization.

It should be noted that the robust control law presented is designed in MATLAB®using double precision (64 bits) floating-point arithmetic. In our case, this control law is embedded in a processor that uses single-precision (32-bit) arithmetic. This circumstance may affect the behavior of the discrete-time closed-loop system. For this reason, the closed-loop system stability in single-precision should be checked after the design.

The properties of the designed controller are discussed in the next section.

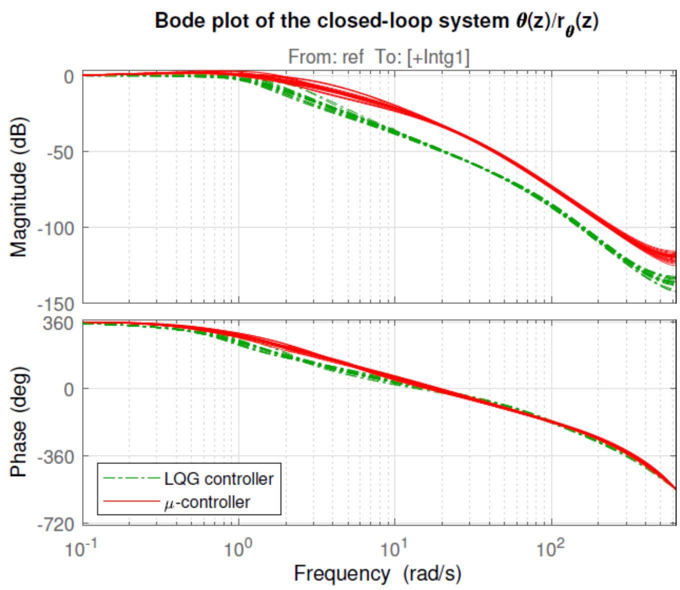

Fig. 13. Bode plot of the uncertain closed-loop system

6. COMPARISON OF THE CLOSED-LOOP SYSTEMS WITH LQG AND μ CONTROLLERS

In this section, we compare the frequency domain properties of the LQG controller and the μ-controller designed in the previous two sections. In the case of μ-controller, we use a 15th-order approximation obtained by the function reduce.

The Bode plot of the closed-loop system is shown in Fig. 13. It is seen that for both controllers, the closed-loop bandwidth is approximately $1\ rad/s$ the μ controller has a wider bandwidth.

The magnitude plots of the tracking errors are shown in Fig. 14. It is seen that the μ controller ensures better attenuation of the tracking error in the frequency range under interest.

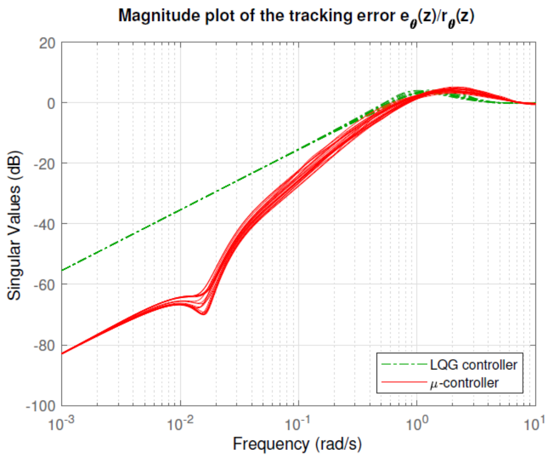

Fig. 14. Magnitude plot of the sensitivity function $S_o G_{r\theta}$

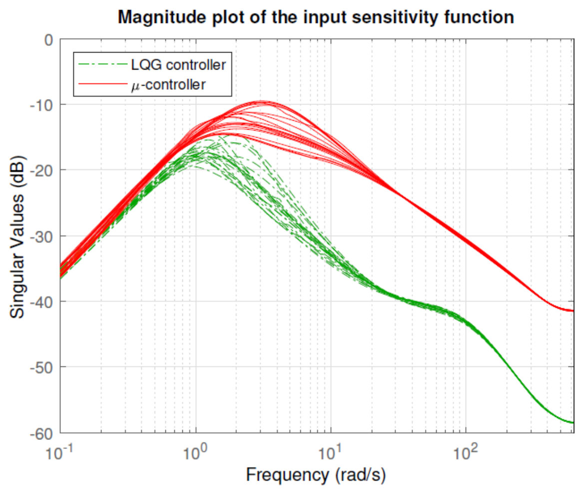

Fig. 15. Magnitude plot of the sensitivity function $S_i K G_{r\theta}$

From the magnitude plots of the input sensitivity function, given in Fig. 15, one may conclude that the LQG controller attenuates better the effect of disturbances and noises in the control action. This is the price to be paid for the wider bandwidth and better tracking in the case of μ controller.

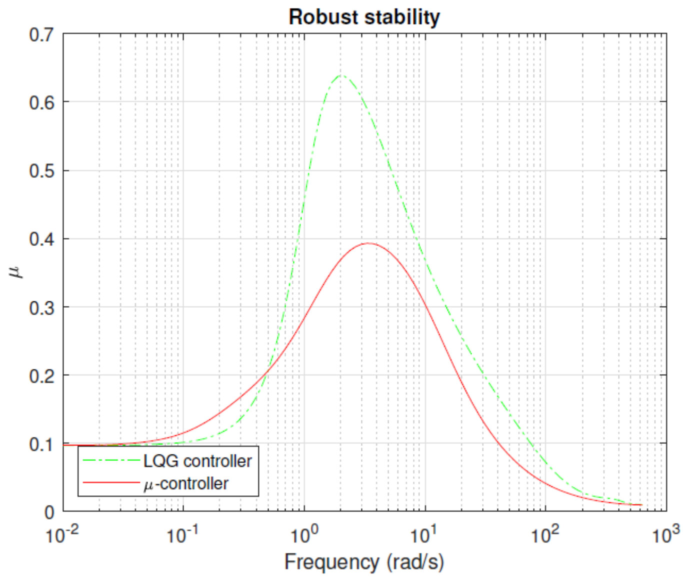

Fig. 16. Robust stability of the closed-loop system

In Fig. 16, we show the plots of upper bounds on the structured singular value corresponding to the robust stability of the closed-loop system for both controllers. The bounds are obtained using the function robuststab from Robust Control Toolbox®3. For each controller, the system achieves robust stability with respect to the uncertainties corresponding to the identification of the robot model. The closed-loop system with μ controller has a better stability margin in comparison to the system with LQG controller, as one may expect.

The robust performance for LQG and μ controllers is shown in Fig. 17. The robust performance analysis is done for the same weighting functions used in the μ-synthesis by using the function robustperf. Not surprisingly, a better performance margin is obtained in the case of the μ-controller, which yields the best performance. It is interesting that in the given case, the LQG regulator with Kalman filter achieves robust performance in the presence of uncertainties corresponding to the identified robot model. This is in contrast with the case of single-input single-output identification reported in [10].

7. EXPERIMENTAL RESULTS

The experimental comparison of the two controllers designed is performed as described in [15] with the aid of the Simulink Coder® tool [14]. The code of the control algorithm is generated by using the Simulink® model. It is implemented in the digital controller as described in [16]. The communication between the computer and the robot controller is performed via the conventional TCP/IP protocol.

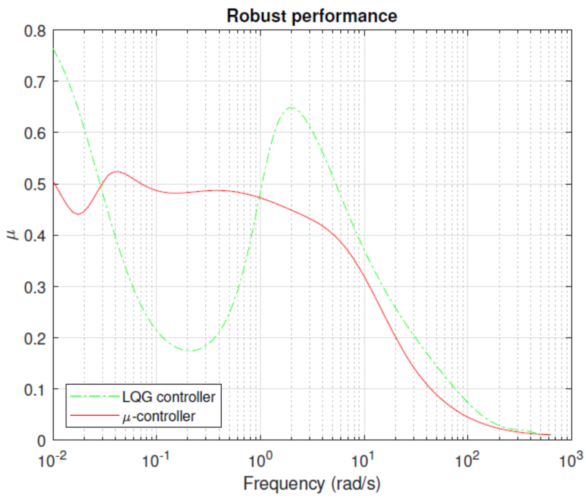

Fig. 17. Robust performance of the closed-loop system

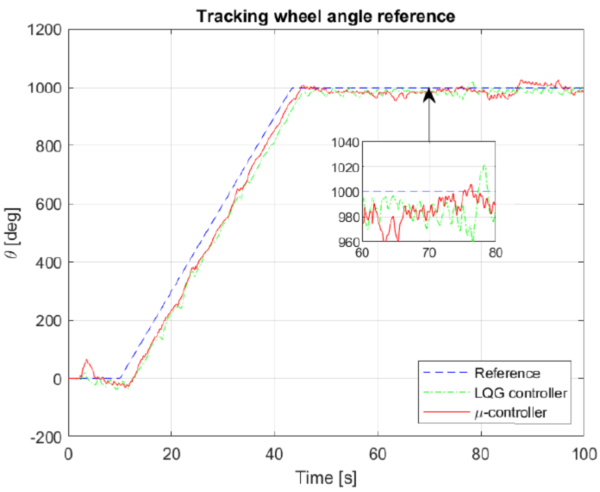

Fig. 18. Tracking wheel angle reference

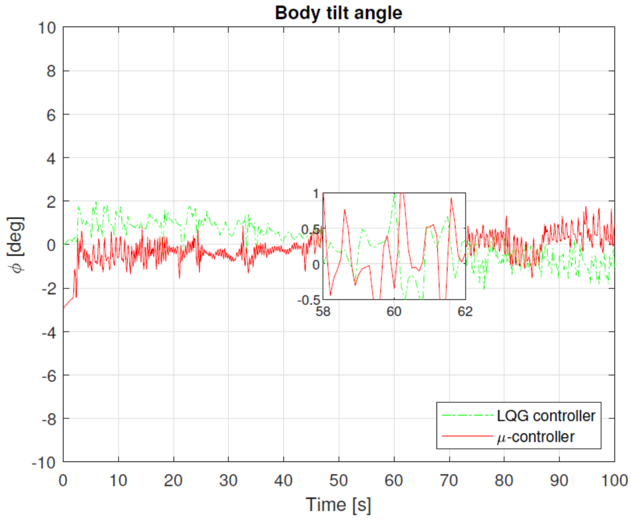

Fig. 19. Tilt body angle

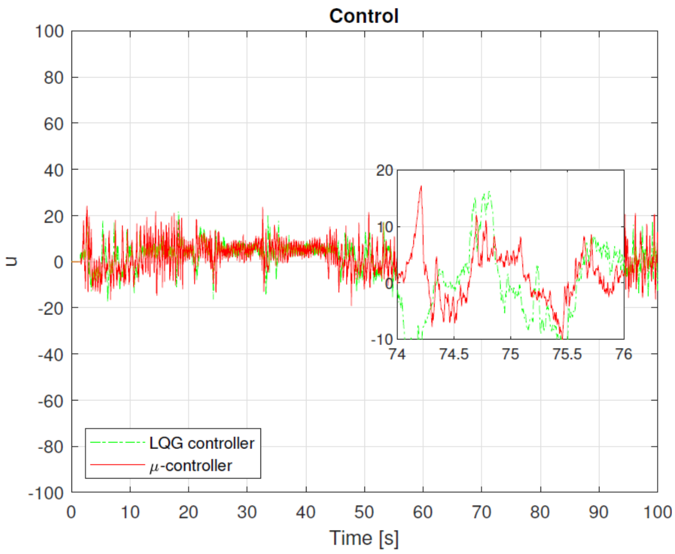

Fig. 20. Control action

The evaluation of the two-wheeled robot control is done for 300 s (60000 samples). The maximum computational time is about $5 \cdot 10^{-5} s$ for both control actions, which is much smaller than the sampling period $T_s = 0.005\ s$.

In Fig. 18, we depict the dynamics of the wheel angle for the two controller algorithms. It is seen that for both controllers, the system has good static performance.

The oscillations that are presented in the tilt body angle are negligible, as seen in Fig. 19.

The experimentally obtained control actions are presented in Fig. 20. As a control action, we consider the duty PWM coefficient that is the input to the DC motors. The maximum control action for both controllers is smaller than 5 units, which is far below the upper allowable bound of 128 units. We note the relatively strong effect of the noise on the control action as a result of the form of the input sensitivity function (Fig. 15).

8. CONCLUSIONS

The comparison of the closed-loop performance of the discrete-time LQG controller with the μ-controller shows that the two controllers have nearly the same properties in the time domain and frequency domain. Also, their properties with respect to the closed-loop robust stability and robust performance are almost the same. The μ-controller is of high order but ensures robust performance for larger parametric perturbations. Both controllers can be used in practice to ensure accurate position tracking and stabilization. The results confirm the advantage of using single-input multi-output models in robot controller design.

9. ACKNOWLEDGMENT

This study is financed by the European Union-NextGenerationEU, through the National Recovery and Resilience Plan of the Republic of Bulgaria, project. BG-RRP-2.004-0005.

REFERENCES

[1] G. BALAS, R. CHIANG, A. PACKARD AND M. SAFONOV, Robust Control Toolbox® 3 User's Guide (2024) Natick, MA: The MathWorks, Inc., online: https://www.mathworks.com/help/pdf_doc/robust/robust_ug.pdf.

[2] Q.-T. DO, V.T. TRAN, M.T. NGO AND AL., Modeling and Optimal Control for Two-Wheeled Self-Balancing Robot (2024) *J. Fuzzy Syst. & Control* **2** (1) 22–28, online: DOI: 10.59247/jfsc.v2i1.162.

[3] F. FERIYONIKA AND A. HIDAYAT, Balancing Control of Two-Wheeled Robot by Using Linear Quadratic Gaussian (LQG) (2020) *Journal of Telecommunication, Electronic and Computer Engineering*, **12** (3) 55–59. ISSN: 2180 – 1843.

[4] J.L. FIGUEROA AND S.I. BIAGIOLA, Modelling and Uncertainties Characterization for Robust Control (2013) *Journal of Process Control*, **23** (3) 415–428, online: DOI: 10.1016/j.jprocont.2012.11.008.

[5] G.F. FRANKLIN, J.D. POWELL AND M. WORKMAN, Digital Control of Dynamic Systems (1998) 3rd ed. Addison Wesley Longman, Inc., Menlo Park, CA. ISBN 0-201-33153-5, online: https://www.researchgate.net/publication/31849881_Digital_Control_of_Dynamic_Systems-Third_Edition.
[6] M. GREWAL AND A. ANDREWS, Kalman Filtering: Theory and Practice with MATLAB®. (2015) 4th ed. John Wiley & Sons, Inc., New York, ISBN 978-1-118-85121-0, online: DOI:10.1002/9780470377819.
[7] D.-W. GU, P. PETKOV AND M. KONSTANTINOV, Robust Control Design with MATLAB® (2013) Springer-Verlag, London, 2nd ed., ISBN: 978-1-4471-4681-0, online: DOI:10.1007/978-1-4471-4682-7.
[8] M. HASSAN, A. MOUSTAFA AND M. MONESS, Modeling and Parameters Estimation of a Self-Balancing Two-Wheeled Vehicle (2024) *Journal of Advanced Engineering Trends* **43** (1) 373–381, online: DOI: 10.21608/jaet.2022.144785.1197.
[9] S. KHATOON, M. ISTIYAQUE, N. HASAN AND D.K. CHATURVEDI, Two-Wheeled Selfbalancing Mobile Robot Using Kalman Filter and LQG Regulator (2021) In: M. Muzammil, A. Chandra, P.K. Kankar, H. Kumar (eds) Recent Advances in Mechanical Engineering. Lecture (pp. 213-221) Notes in *Mechanical Engineering. Springer, Singapore,* online: DOI: 10.1007/978-981-15-8704-7_26.
[10] J. KRALEV, TS. SLAVOV AND P. PETKOV, Design and Experimental Evaluation of Robust Controllers for a Two-Wheeled Robot (2016) *International Journal of Control*, **89** (11) 2201-2226, online: DOI: 10.1080/00207179.2016.1151940.
[11] L. LJUNG, System Identification: Theory for the User (1999) *IEEE Robotics & Automation Magazine,* **19** (2) Prentice-Hall, Inc., Englewood Cliffs, NJ, 2nd ed. ISBN: 978-0136566953, online: DOI:10.1109/MRA.2012.2192817.
[12] L. LJUNG, System Identification Toolbox®User’s Guide (2022) The MathWorks Inc., Natick, MA, online: https://www.mathworks.com/help/pdf_doc/ident/ident_ug.pdf.
[13] A. MISHRA AND K. BANSAL, Control of Two-Wheel Self-Balancing Robot: LQR and MPC Performance Analysis (2024) IEEE Int. Students’ Conf. Electrical, Electronics and Computer Science (SCEECS), 24-25 Feb. 2024, Bhopal, India, online: DOI: 10.1109/SCEECS61402.2024.10481856.
[14] SIMULINK CODER, The MathWorks (2021). Inc., Natick, MA, online: https://www.mathworks.com/help/pdf_doc/rtw/rtw_ug.pdf.
[15] P. PETKOV, T. SLAVOV AND J. KRALEV, Design of Embedded Robust Control Systems Using MATLAB/Simulink (2018) IET Control, Robotics and Sensor Series 113. The IET, London, ISBN 978-1-78561-330-2, online: DOI:10.1049/PBCE113E.
[16] RASPBERRY PI 4 MODEL B (2021). Raspberry Pi (Trading) Limited, Cambridge, UK. online: https://www.raspberrypi.org/products/raspberry-pi-4-model-b/.
[17] S. SKOGESTAD AND I. POSTLETHWAITE, Multivariable Feedback Control (2005) 2nd ed. John Wiley and Sons Ltd, Chichester, UK, ISBN: 978-0-470-01167-6, online: https://www.researchgate.net/publication/229058308_Multivariable_Feedback_Control_Analysis_and_Design.
[18] T. SLAVOV, J. KRALEV AND P. PETKOV, Linear Quadratic Control of a Two-Wheeled Robot (2014) Comptes rendus de l’Acad´emy Bulgare des Sciences, **67** (8) 1153–1158, online: http://www2.coe.pku.edu.cn/tpic/file/20181026/20181026214635993599.pdf.

[19] T. SLAVOV, J. KRALEV, P. PETKOV AND S. SHERIF, Multi-Output Identification and LQG Control of a Two-Wheeled Robot (2021) International Conference ICAI, 30 Sept. - 2 Oct. 2021, Varna, Bulgaria. IEEE, online: DOI:10.1109/ICAI52893.2021.9639736.
[20] T. SLAVOV, J. KRALEV AND P. PETKOV, Multi-Output Identification and Robust Control of a Two-Wheeled Robot (2023) 9 th International Conference CoDIT, 3-6 July 2023, Rome, Italy. IEEE. online: DOI:10.1109/CoDIT58514.2023.10284299.
[21] K. ZHOU, J. DOYLE AND K. GLOVER, Robust and Optimal Control (1996) Prentice Hall, Upper Saddle River, NJ, ISBN: 0-13-456567-3, online: https://www.academia.edu/522477/Robust_and_optimal_control#loswp-work-container.

Received May 4, 2025